sustainability

MDPI

Article

Flood Risk Mapping during the Extreme February 2021 Flood in the Juruá River, Western Brazilian Amazonia, State of Acre

José Mantovani [1,2], Enner Alcântara [1,2,*], José A. Marengo [2,3], Luciana Londe [2,3], Edward Park [4], Ana Paula Cunha [2,3] and Javier Tomasella [2,5]

1 Institute of Science and Technology, São Paulo State University (Unesp), São José Dos Campos 12245-000, SP, Brazil; j.mantovani@unesp.br
2 Graduate Program in Natural Disasters, (Unesp/CEMADEN), São José Dos Campos 12247-004, SP, Brazil; jose.marengo@cemaden.gov.br (J.A.M.); luciana.londe@cemaden.gov.br (L.L.); ana.cunha@cemaden.gov.br (A.P.C.); javier.tomasella@inpe.br (J.T.)
3 National Center for Monitoring and Early Warning of Natural Disasters (CEMADEN), São José Dos Campos 12247-016, SP, Brazil
4 National Institute of Education, Earth Observatory of Singapore and Asian School of the Environment, Nanyang Technological University (NTU), Singapore 639798, Singapore; edward.park@nie.edu.sg
5 National Institute for Space Research (INPE), Cachoeira Paulista 12630-000, SP, Brazil
* Correspondence: enner.alcantara@unesp.br

Abstract: Cruzeiro do Sul, a municipality in Northwestern Brazil is recurrently impacted by floods, particularly along the Juruá River. This study presents a comprehensive flood risk analysis by integrating geoprocessing, remote sensing, and hydraulic modeling techniques. Our objectives are to simulate flood extents, identify high-risk areas, and guide sustainable territorial management. Our findings illustrate that the flood impacts are distributed across urban (27%), agricultural (55%), and forest/grassland (17%) landscapes. Historical records and literature reviews also underscore a recurring pattern of extreme floods in the municipality, notably during February's La Niña events. Some vulnerable urban neighborhoods were identified: Vila Cruzeirinho, Centro, Miritizal, and Da Várzea. These areas are especially susceptible due to their proximity to the river and increased surface runoff during high flood events. By amalgamating various data sources and methods, this research aids decision making for flood mitigation and urban development, fostering resilience against recurrent flooding events in Cruzeiro do Sul.

Keywords: natural hazards; floods; remote sensing; environmental modeling; Brazil

Citation: Mantovani, J.; Alcântara, E.; Marengo, J.A.; Londe, L.; Park, E.; Cunha, A.P.; Tomasella, J. Flood Risk Mapping during the Extreme February 2021 Flood in the Juruá River, Western Brazilian Amazonia, State of Acre. *Sustainability* **2024**, *16*, 2999. https://doi.org/10.3390/su16072999

Academic Editor: Tommaso Caloiero

Received: 1 March 2024
Revised: 26 March 2024
Accepted: 1 April 2024
Published: 3 April 2024

1. Introduction

The need to address the global challenges presented by disasters has never been more urgent. Out of these, floods stand out as the most common and damaging natural events, affecting billions of people and causing enormous economic losses worldwide [1]. In Brazil, flooding is a particularly pressing issue that often results in irreparable losses for affected populations [2,3]. The country's unique geographical and climatic variables contribute to a landscape inherently prone to such catastrophes. The rainy season in the northern region of Brazil varies depending on the subregion, but it typically occurs from December to May, during which flood events become more frequent. Rivers swell due to increased rainfall, impacting human settlements along their banks. The situation is further complicated in the Amazon region, where large scale climatic phenomena like the Intertropical Convergence Zone (ITCZ) and the La Niña climatic phenomena play a significant role in exacerbating flood risks [4–6]. This increased susceptibility raises questions about best practices to manage flood risks and protect vulnerable communities in a region of such environmental and climatic complexity.

The challenges of flood management are further exacerbated by the patterns of urban development commonly found in Brazil and other developing countries. Historically, many

Brazilian cities have been established along riverbanks and water sources. These areas are ideal for agriculture, provide critical water resources, and, in some cases like the Amazon, are crucial for transportation where land travel is often logistically challenging. However, unchecked expansion into these areas, together with inadequate planning or environmental considerations, compromises their natural role as floodwater buffers. As a result, cities have become increasingly vulnerable to flooding, heightening the urgency for better spatial planning and more sustainable approaches to urban development.

Until now extensive research has been conducted to understand flood patterns and develop effective flood management strategies. Technologies like geographic information systems (GIS), remote sensing, and hydraulic modeling platforms like HEC-RAS have been at the forefront of these efforts [7–13]. These studies offer vital insights into flood risk assessment and contribute significantly to disaster preparedness. However, a limitation of existing research is the predominant focus on regions different from the Amazon. The unique hydrological, climatic, and geographical features of the Amazon demand specialized studies tailored to its specific challenges. Challenges in Amazon research include remote terrain with dense vegetation and limited infrastructure, extreme environmental conditions affecting fieldwork, and the immense biodiversity requiring specialized expertise. Additionally, health risks from venomous animals and infectious diseases, coupled with political and socioeconomic dynamics and environmental threats like deforestation and climate change, create further barriers for researchers.

One area where the impact of these variables comes sharply into focus is Cruzeiro do Sul, a city that lies along the banks of the Juruá River in the Amazon region. This city has grappled with frequent and severe flooding events, often catalyzed by the natural seasonal dynamics and exacerbated by larger climatic phenomena like La Niña (Civil Defense, COMDEC). As a vital urban center in the state of Acre (AC, State abbreviation), Cruzeiro do Sul's vulnerability to floods carries broad repercussions. For example, the last major flood in February 2021 led to a state of emergency, affecting around 33,000 people, and causing widespread damage. Infrastructure such as roads, bridges, and public utilities were significantly impaired, causing ripple effects across essential services like healthcare and emergency response. Neighborhoods such as Vila Cruzeirinho, Centro, Miritizal, and Da Várzea are particularly at risk, given their immediate proximity to the Juruá River. This alarming pattern does not merely disrupt everyday life; it also poses long-term challenges for the socioeconomic well-being of the region, impacting everything from local commerce to educational facilities. The complexity of the situation is such that purely responsive measures are insufficient, hence the need for an in-depth scientific analysis to support future disaster mitigation efforts.

In this study we aim to address a pressing gap in the existing body of literature by assessing the flood dynamics in Cruzeiro do Sul. While other studies have utilized technology such as geoprocessing techniques, remote sensing, and hydraulic models for flood management, none have yet tailored these approaches to the unique set of challenges posed by the Amazonian hydrological and climatic conditions. Many parts of the Amazon lack infrastructure, including monitoring stations and gauges, which are essential for collecting real-time data on water levels and rainfall. This makes it difficult to monitor and predict flood events accurately. By combining these techniques, this study provides a comprehensive understanding of the flood risk landscape in Cruzeiro do Sul.

Furthermore, the identification of vulnerable urban neighborhoods and the historical analysis of extreme floods, particularly during La Niña events in February, adds valuable insights into the recurring nature of flood events in the area. Overall, the integration of geoprocessing, remote sensing, and hydraulic modeling methods enables a holistic approach to flood risk assessment, aiding in decision making for flood mitigation and urban development planning. This interdisciplinary approach fosters resilience against recurrent flooding events in the municipality, making it a significant innovation in addressing flood risk management.

Therefore, the primary objective of this research is to deploy an integrated methodology that synthesizes these technologies to yield actionable insights specific to Cruzeiro do Sul and, by extension, the Amazon. By combining these technologies, this study aims to create detailed flood maps, identify high-risk zones, and make specific policy recommendations for adaptive and sustainable flood management strategies. In achieving these aims, this research will serve dual purposes: firstly, to enhance the scientific understanding of flood patterns and risks in unique ecosystems such as the Amazon and secondly, to offer empirically grounded advice to local governments, policymakers, and community stakeholders. Thus, this research endeavors not just to advance academic discourse but also to yield tangible benefits for communities most directly impacted by flooding in the region.

Study Area

The area of the municipality is 7924.94 km^2 and the urban area is 24.794 km^2. It borders the state of Amazonas (to the north) and the municipalities of Porto Walter-AC (to the south), Tarauacá-AC (to the east), and the municipalities of Mâncio Lima-AC, Rodrigues Alves-AC and the neighbor country Peru (to the west). According to the Brazilian Institute of Geography and Statistics [14], Cruzeiro do Sul is the second most populous municipality in the state, with a population of 91.888 inhabitants according to the 2022 Demographic Census estimates. Cruzeiro do Sul is bathed by the Juruá River, with muddy, navigable waters. This river originates in Peru and is 2410 km in length (Figure 1). The study area is formed by a relief geomorphology characterized by a series of hills and flat areas, composed by predominantly Amazonian vegetation [15]. The climate is characterized as equatorial (type "Af" in the Köppen–Geiger climate classification) [16], hot, and humid, with an average annual temperature of around 25 °C and annual rainfall greater than 2000 mm.

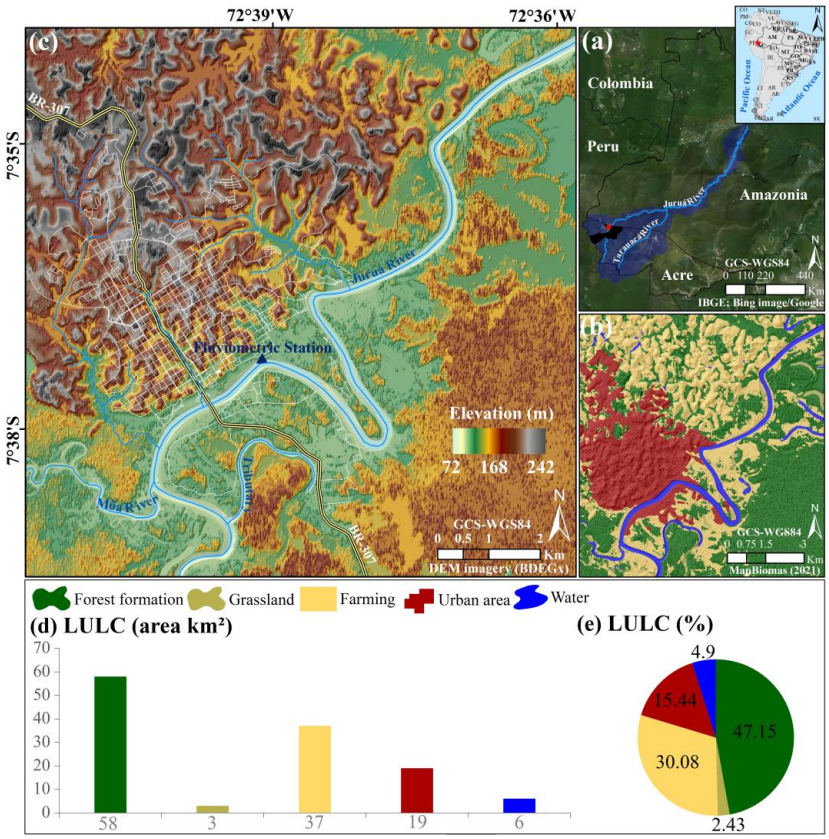

Figure 1. (**a**) Location of study site in Brazil, highlighting the Taquari-Antas basin; (**b**) land use and land cover for Cruzeiro do Sul (Acre State, Brazil); (**c**) Digital Elevation Model (MDE) for the study area with road network superimposed and the position of the Fluviometric station (Source: National Water Agency—ANA); (**d**) land use and land cover (LULC) area in km^2; and (**e**) LULC in %.

The Juruá River is a river that originates in Peru, flows through the states of Acre and Amazonas, and empties into the Solimões River, covering approximately 3000 km. It holds significant importance for the region, serving as a waterway for various communities, since roads are largely absent along most of its course. Important municipalities like Eirunepé in Amazonas and Cruzeiro do Sul, the second-largest city in the state of Acre, are situated along its banks. There is a history of recurrent floods and inundations in the Juruá River, particularly in the section that passes through the municipality of Cruzeiro do Sul. According to data from COMDEC (Civil Defense), as released by the Fire Department, the last major flood was recorded in February 1995 when the river's level reached 14.18 m. In 2017, also in the month of February, the river's level exceeded the previous record set 22 years prior (1995), reaching 14.20 m. In February 2021, another flooding event occurred in Cruzeiro do Sul. Around 33,000 people were affected by the flooding of the Juruá River and its tributaries after the Juruá River reached a record level of 14.31 m on 19 February, surpassing the previous maximum of 14.24 m recorded in February 2017. The state declared a state of emergency.

2. Materials and Methods

Figure 2 illustrates the comprehensive flow diagram that delineates the process of mapping the risk of flooding within the designated study site. This flow diagram illustrates the step-by-step process employed to obtain the map of flood risk within the study site.

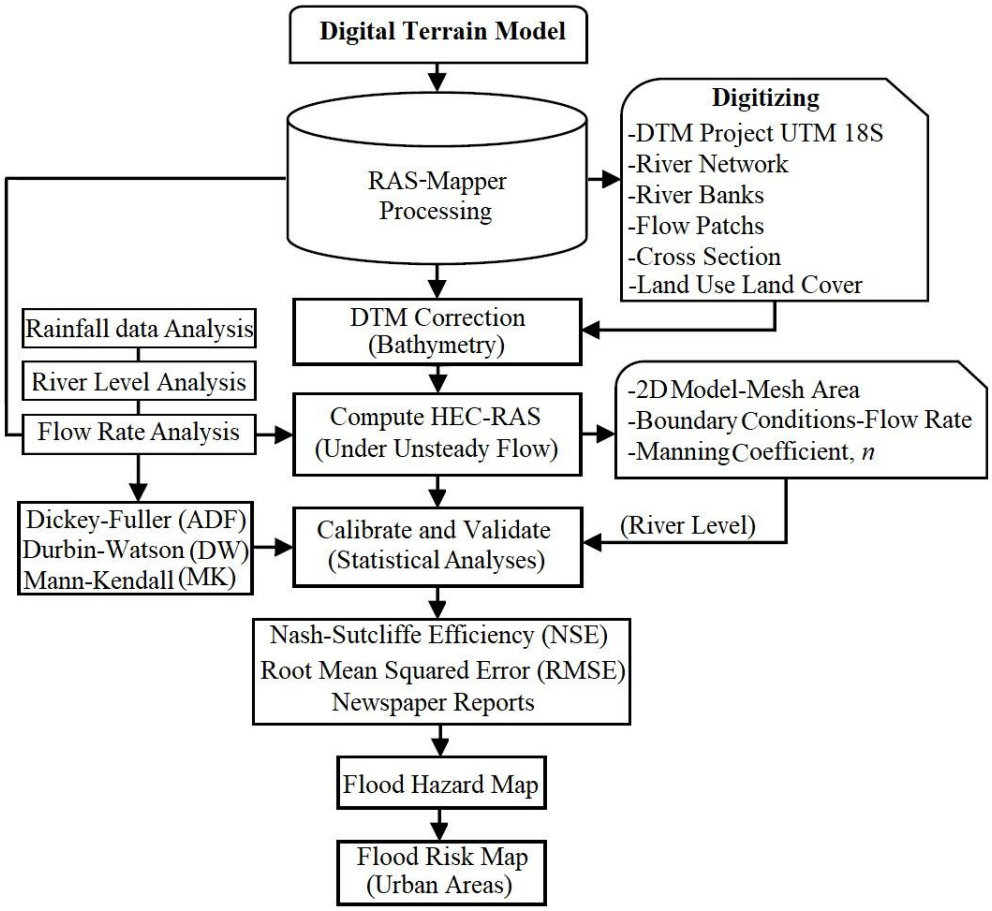

Figure 2. Flow diagram to obtain the map of flood risk in the study site.

The diagram begins with data acquisition, including geographical and hydrological data, which serves as the foundation for subsequent analysis. Following data acquisition, preprocessing steps such as data cleaning and quality control are conducted to ensure the accuracy and reliability of the data. The rainfall data were initially utilized to understand

the climatic conditions within the urban area under study. Statistical methods were then applied to analyze the trends observed in the rainfall data. However, in the context of estimating urban flooding, a decision was made not to directly incorporate the rainfall data into the model. Instead, the focus shifted towards utilizing data pertaining to water level and flow rate. This decision was likely driven by the recognition that factors such as water level and flow rate have a more direct and immediate impact on urban inundation dynamics, thus warranting their prioritization in the modeling process. The next stage involves data integration and analysis, where various methods such as geoprocessing, remote sensing, and hydraulic modeling techniques are applied. Geoprocessing techniques are utilized to manipulate and analyze spatial data, while remote sensing data provide valuable information on land cover and flood extent. Hydraulic modeling techniques are then employed to simulate flood extents and assess flood risk within the study area. Once the analysis is completed, the results are synthesized and interpreted to generate the flood risk map. This map highlights areas of varying flood risk levels, ranging from low to high risk, based on the analysis conducted. Finally, the flood risk map is validated using historical flood data and ground truthing, ensuring its accuracy and reliability for decision-making purposes.

2.1. Data

2.1.1. Rainfall Time Series

This study uses a wide range of data sources, from observational (rainfall data, flow rate data, and river level data) as well as gridded data sets, namely a Digital Elevation Model (DEM), a radar image using the P band with a spatial resolution of 5 m, from the Directorate of Geographic Service [17] and the Army Geographical Database (BDGEx). With respect to the dataset for the analysis of hydrological data, we used fluviometric data from the National Water Agency (ANA), station Code 12500000, located on the edge of Juruá River in the municipality of Cruzeiro do Sul-AC (Lat: -7.63° and Long: -72.66°), with time-series data covering the years from 1981 to 2019. The historical series used was chosen due to the availability of flow- and river-level data at the station up until 2019. For analysis of rainfall data, the same location as the ANA station was selected, using data from the Climate Hazards Group InfraRed Precipitation with Station data (CHIRPS) dataset [18]. CHIRPS is a rainfall product available at daily to annual time scales with a spatial resolution of $0.05^{\circ} \times 0.05^{\circ}$, covering the years from 1981 to 2019, available at https://data.chc.ucsb.edu/products/CHIRPS-2.0/, accessed on 2 February 2021.

The hydrological time series underwent analysis using a box plot approach, with subsequent statistical analyses applied to discern patterns and relationships among the dataset's variables for the calibration of the 2D model. Seasonality was assessed through the Augmented Dickey–Fuller (ADF) test, while autocorrelation was examined using the Durbin–Watson (DW) and Mann–Kendall tests [19]. The Mann–Kendall test, a robust nonparametric method, was employed to identify significant time trends, with the ADF test evaluating stability and seasonality presence. The DW test, suitable for nonlagged dependent variables and small sample sizes, assessed autocorrelation [20,21]. Trend analysis facilitated the identification of behavioral changes over time, and Theil–Sen Robust Linear Regression (TS) validated time-series trends using a median-based, outlier-resistant approach [22]. The resultant statistical analyses informed the calibration of the flood model for 19 February 2021.

2.1.2. Rainfall Anomalies

Monthly rainfall anomalies (mm), accumulated rainfall in February 2021, and accumulated rainfall from 13 to 20 February 2021 was obtained from the Multisatellite Precipitation Retrieval and Evaluation for Global Precipitation Measurement (MERGE) dataset. The MERGE rainfall product incorporates data from various satellite sensors and sources, including infrared and microwave sensors, to estimate precipitation rates over different regions of the Earth. By merging data from multiple satellites, the product aims to over-

come limitations associated with using a single satellite sensor and provide a more reliable representation of rainfall [23,24].

2.1.3. Land Use and Land Cover (LULC) Data

A map of Land Classification Layers (LULC) was also used, with data from the MapBiomas Project of 2019 (Figure 1b), collection 7 (available in https://mapbiomas.org/en?cama_set_language=en, accessed on 2 February 2021) [25]. The urban mesh data were also used in shapefile format referring to the municipality, obtained from the OpenStreetMap (available in http://download.geofabrik.de, accessed on 2 February 2021), for qualitative and quantitative analysis that corroborates the impacts of observed rainfall extremes on floods.

2.1.4. Digital Elevation Model

A primary challenge in hydraulic modeling arises from the frequent absence of bathymetric data in terrain datasets. A crucial element for constructing an accurate river hydraulics model is an adequate depiction of ground surface elevations, particularly for analyzing river and floodplain regions. A well-crafted terrain model precisely delineates the elevations of river channels and floodplains, integrating key features that influence water flow, including channel bottoms, banks, and elevated structures such as roads and levees [26]. The DEM derived from radar image (DEM, 5 m of spatial resolution) does not have the bathymetry data for the channels. However, the correction of the DEM was carried out and the bathymetry was created based on data from the fluviometric station via ANA of Juruá River, Cruzeiro do Sul. Thus, a 1D model was created for the channel part of the terrain surface, using the river centerline, cross sections and bank lines, using RAS Mapper [27] to create an interpolated surface of channel. Thus, a new DEM was created that combines the surface along the channel (with maximum priority) with the radar-derived DEM [28,29].

2.2. Methods

2.2.1. Flood Inundation Modeling

This study began by gathering relevant data, including geographical, hydrological, and remote sensing data, which are essential for understanding the flood dynamics in Cruzeiro do Sul. Before the flood risk analysis, the acquired data were subjected to preprocessing steps such as cleaning, validation, and interpolation to ensure data quality and reliability. This study integrates geoprocessing, remote sensing, and hydraulic modeling techniques. Geoprocessing is used for spatial data analysis, remote sensing for land cover mapping and flood extent estimation, and hydraulic modeling for simulating flood extents and impacts. Clear objectives are outlined, including simulating flood extents, identifying high-risk areas, and guiding sustainable territorial management. These objectives guided the setup and calibration process of the flood risk model. This study analyzes the findings, highlighting the distribution of flood impacts across different landscapes, and identifies vulnerable urban neighborhoods. This analysis provides insights into flood dynamics and informs decision-making processes. The flood risk model is calibrated to ensure its accuracy and reliability. This process involves adjusting model parameters based on historical records and literature reviews to better simulate extreme flood events, such as those associated with La Niña events in February. Model validation is conducted to assess the reliability of the flood risk model's predictions. This validation involves comparing model outputs with observed flood events and historical data to ensure that the model accurately represents the real-world flood dynamics in Cruzeiro do Sul.

We simulate the flood events from 1 February to 28 February 2019. using fluviometric data from ANA. The software used for flood mapping was HEC-RAS 6.2. The model is based on solving one- or two-dimensional Saint-Venant equations, considering steady or unsteady flow (dynamic) regimes. HEC-RAS was chosen for mapping flooding due to its established reputation for accurately simulating river hydraulics and flood extents (United

States Army Corps of Engineers) [30]. Its capabilities in representing complex riverine systems, including the intricate network of channels and floodplains characteristic of the Amazon region, make it a suitable tool for this purpose [31]. Additionally, HEC-RAS allows for the integration of various data sources, such as topographic surveys and hydraulic parameters, enabling a comprehensive analysis of flood risk in the study area [32]. Its widespread use in hydrological studies and its ability to generate detailed flood inundation maps make it an appropriate choice for accurately depicting the extent and magnitude of flooding events in the Amazon [33]. Previous studies have also demonstrated the effectiveness of HEC-RAS in flood routing simulation and inundation mapping in different regions [34].

In this study, mapping was performed using the unsteady flow method which enabled recreating the event that occurred on 19 February 2021. Under unsteady flow, the user inputs a discharge hydrograph at the upstream boundary and a discharge-stage rating at the downstream boundary. In typical projects of limited channel lengths, a kinematic wave, which keeps its discharge constant, is a better assumption than a dynamic wave, which attenuates its discharge [35].

The input data for elaboration of 2D models were channel topography, mesh area, boundary conditions through flow rate data (of the main channel and the two tributaries (Figure 1c), an output condition, and the Manning coefficient, *n*. The boundary conditions adopted for modeling the event that occurred were based on daily flow data for the month of February, from the 1st to the 28th, 2021, to recreate the last flood event, since the transshipment of river level for the year 2019, according to information from the local press, was the same as for the year 2021 (14.36 m). LULC classes (MapBiomas Project) were used to identify specific parameter values for Manning's coefficient *n* values for each cell of the DEM. The values of Manning coefficient, *n*, are shown in Table 1.

Table 1. Manning's *n* roughness values associated with different land covers for the low, medium, and high ranges.

Land Cover	Manning's *n*
Forest formation	0.06
Grassland	0.04
Farming	0.04
Water bodies	0.035
Urban area	0.07
Main channel	0.035

Although we cannot say for certain which Manning's *n* values best characterize the actual conditions of the study areas, because Manning's *n* has no independent physical basis, the values tested are within the ranges commonly used in flood modeling available in the literature [36].

2.2.2. Mapping Urban Areas at Risk

A risk map was generated through the intersection of the urban mesh with the flood map. For this, the flood map was reclassified into 5 classes, stratified into risks: Lower, Less, Medium, High, and Very-High. The criterion established to determine the classes consisted of the river level (under alert) to the highest levels of the river (overflow) and the maximum level reached by the river flooding. The classification of risks has been allocated following the methodology of the Ministry of Land and Transportation MLT of Japan [37], adapted by [38], as shown in Table 2.

Table 2. Classification of MTL flood risks.

Flood	Depths (m)	Juruá River	Risk
F1	<12.8	Below the trans-shipment quota	Lower
F2	13.0	Trans-shipment quota	Less
F3	13.6	Above the transfer quota	Medium
F4	14.1	Far above the trans-shipment quota	High
F5	14.36	Extremely over the trans-shipment quota	Extreme

The annual fluctuation of the river level in its middle section ranges from 12 to 13 m. Generally, the Juruá River floods its plains from December to mid-May. The highest water levels, exceeding the overflow level (13 m), reach a maximum value of 14.36 m. Five risk classifications have been determined: F1, F2, F3, F4, and F5. The F1 risk (less than 12.8 m deep) is permitted, as people can easily evacuate on foot, situated in areas far from the Juruá River. The F2 risk (depth of 13 m) is also considered low risk, as it is located in areas distant from the river, allowing for the evacuation of adults and children in this area. The F3 risk (depth of 13.6 m) is a moderate-risk zone where people can drown, but they are safe up to 0.6 m, albeit with considerable risk. The F4 risk (depth of 14.1 m) is a high-risk zone where residents in this area are not protected in their homes but may find safety on their rooftops when possible. The F5 risk (depth exceeding 14.36 m) is an extremely dangerous zone where even on their rooftops, citizens are not protected [38].

A graph also was created from the stratified classes with the areas of the flood patch, only for the urban perimeter. The annual fluctuation of the river level in its median stretch varies from 12 to 13 m. In general, the Juruá River floods its plains from December to mid-May. The highest values of quotas, above the trans-shipment quota (13 m), with a maximum value of 14.36 m. All sets of data were organized in HEC-RAS/RAS MAPPER software version 6.3 to simulate the event. Posteriorly, the analysis of results was carried out in a GIS environment using the software ArcGIS Pro (ESRI).

2.2.3. Model Performance Evaluation

To calibrate and validate the model and for comparison purposes, quantitative information is required to measure model performance. In this study, to validate and assess the results generated with the model, we used observed data from river levels extracted from the fluviometric station and data generated with the model. The selected period consisted of 1 day after the event (21 February 2021), from the 22nd to the 28th; during and after calibration, we used two statistical indicators to evaluate the existence of systematic errors: the Nash–Sutcliffe efficiency (NSE) and the RMSE-observations standard deviation ratio (RSR).

The Nash–Sutcliffe efficiency (NSE) is used to assess the predictive skill of hydrological models. It consists of a normalized statistic that determines the relative magnitude of the residual variance ("noise") compared to the measured data variance ("information") [39]. The NSE indicates how well the plot of observed versus simulated data fits the 1:1 line. It is defined as Equation (1):

$$NSE = 1 - \frac{\sum_{t=1}^{T}\left(Q_0^t - Q_m^t\right)^2}{\sum_{t=1}^{T}\left(Q_{0-}^t \overline{Q}_0\right)^2} \quad (1)$$

where (Q_0) is the mean of observed discharges, and Q_m is modeled discharge. Q_0^t is observed discharge at time t.

The Nash–Sutcliffe efficiency (NSE) is calculated as 1 minus the ratio of the error variance of the modeled time series to the variance of the observed time series. An NSE of 1 indicates a perfect model, while an NSE of 0 means the model is no better than the mean of the time series in terms of prediction. Negative NSE values indicate that the observed mean is a better predictor than the model. NSE values closer to 1 suggest greater

predictive skill of the model. Different authors have proposed NSE values as thresholds of sufficiency. Subjective application of different NSE values as thresholds of sufficiency have been suggested by several authors [40–42].

The root-mean-square deviation (RMSD) measures the average size of discrepancies between predicted and observed values. It is used to assess the accuracy of forecasting models within a dataset. RMSD is always non-negative, with lower values indicating better accuracy. However, it is important to note that RMSD comparisons between datasets are unreliable due to its scale dependency [43].

The RMSE-observations standard deviation ratio (RSR) is determined by dividing the RMSE by the standard deviation of the measured data. The RSR ranges from an optimal value of 0 to a higher positive value. A lower RSR corresponds to a lower RMSE and indicates better performance in model simulation. The RSR standardizes the root-mean-square Error (RMSE) by incorporating the standard deviation of observed values. It goes from an optimal value of 0 to infinity. Based on the RSR, [42] indicates performance ratings as follows: (i) very-good (0–0.50); (ii) good (0.50–0.60); (iii) satisfactory (0.60–0.70); or (iv) unsatisfactory (>0.70). It is defined as Equation (2):

$$RSR = \frac{1}{n}\sum_{i=1}^{n}(P_i - O_i)^2 \quad (2)$$

where P_i is the predicted value and O_i is the observed value.

After the calibration and validation steps, the results were analyzed statistically and spatially, with maps and graphics.

3. Results

3.1. Climate, Hydrology, and Impacts of the Floods in Acre in February 2021

In central Amazonia [44,45] in December 2020–February 2021 precipitation was about 200–250 mm above normal (relative to 1981–2010). In the Brazilian Amazon, 583.8 mm of precipitation were registered for Manicoré in March (the normal is 300 mm) and 604 mm were registered for Tucuruí (the normal is 436.7 mm). During February of 2021, heightened precipitation targeted the Acre state, resulting in significant flooding within its municipalities, as well as impacting cities in Amazonas adjacent to the area, including Ipixuna, Boca do Acre, and Envira. By March, a classification of rainfall ranging from very wet to extremely wet was documented across the entirety of the western Amazon region [46]. Figure 3 shows that rainfall in western and central Brazilian Amazonia, including the Peruvian and Northern Bolivian Amazonia, was well above 150–250 mm above normal in February 2021 (Figure 3a), with values reaching 450 mm or more over those regions, as accumulated in February (Figure 3b). In these regions, during 13–20 February 2021, accumulated rainfall was above 200 mm, almost 50% of the accumulated monthly levels (Figure 3c).

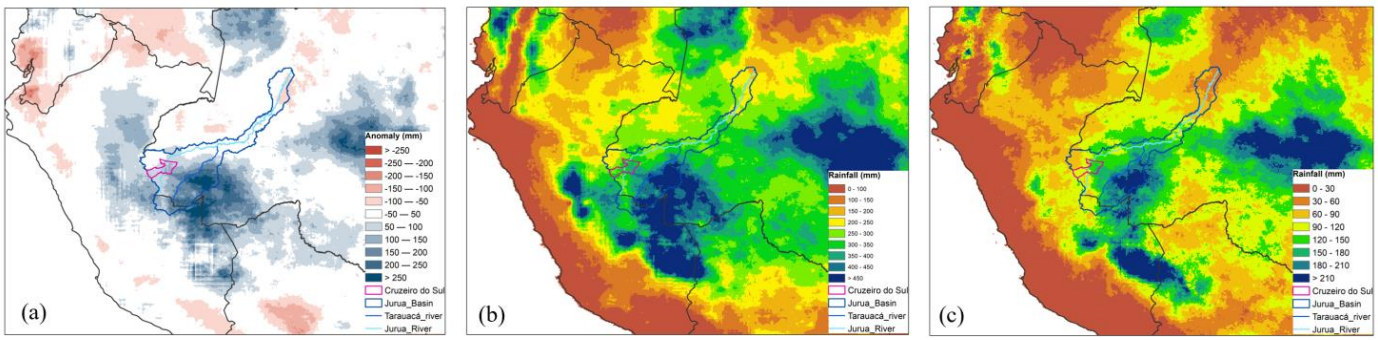

Figure 3. (**a**) Monthly rainfall anomalies (mm), (**b**) accumulated rainfall in February 2021, and (**c**) accumulated rainfall from 13 to 20 February 2021.

Spatial dependence is evident in the anomalies, particularly notable in the western sub-basins like the Solimões River, which encountered significant anomalies in early 2021. Notably, flooding occurred in the Peruvian Amazon from 13 to 20 February 2021, with the Iñapari River's flow peaking at 29,601.6 m^3/s on 20 February 2021, surpassing the previous record set on 3 March 2017, at 18,357.2 m^3/s. On 13 February, flooding was reported along the Pukiri and Colorado Rivers and on 15 February 2021 along the Tahuamanu River in the Bolivian Amazon. In Naranjitos, Amazonas state, the Utcubamba River's flow exceeded the flood limit of 394.3 m^3/s, reaching 673.8 m^3/s on 12 February 2021. In Rio Branco, the capital of the state of Acre, the Acre River reached 15.77 m on 17 February, 2 m above the critical flood level. Meanwhile the Acre River stood at 15.64 m as of 20 February, above the flood stage of 14 m [47]. By 23 February 2015, the Acre River overflowed, and heavy rainfall on 3 and 4 March had forced river levels higher still, and by 4 March levels of the Acre River reached a record 18.40 m.

The floods that affected the state in the second half of February 2022 were considered historical records and affected about 118,000 people, and more than 10,000 were affected by power shortages. The current flood situation has been described as the worst in 132 years [48]. In the city of Cruzeiro do Sul, the second largest city in the state of Acre, floods of the Juruá river reached 13.21 m on 14 February, 13.84 m on 15 February, 14.31 m on 19 February (beating the previous high of 14.24 m set in February 2017), 14.31 m in February 2021, and 14.02 m on 24 February. The critical level for floods is 11.8 m. The levels of the Juruá River were considered the highest ever recorded [49].

By 16 February 2021 the governor of Acre decreed emergency because of the floods in the cities of Santa Rosa do Purus, Feijó, Tarauacá, Jordão, Cruzeiro do Sul, Sena Madureira, Rio Branco, Porto Walter, and Mâncio e Rodrigues Alves. By 20 February 2021, according to the Agencia Brasil news (https://agenciabrasil.ebc.com.br/geral/noticia/2021-02/acre-continua-sofrer-com-cheias dengue-e-COVID-19, accessed on 20 February 2021), in the state of Acre more than 130,000 people were affected by the floods, in the capital Rio Branco and in small cities. The floods were caused by the flooding of the Acre, Juruá, Envira, Iaco, and Purus rivers, in addition to springs and streams. The Purus River reached 9.69 m on 19 February, 11 cm lower than on 18 February, and on 17 February the river reached 10.03 m. In the city of Cruzeiro do Sul, almost 40,000 people were affected, while in Tarauacá the number was 28,000, and in the capital, Rio Branco, 25,000 people were affected. In addition to the floods, the state was also facing a migratory crisis, dengue outbreaks, and a lack of intensive-care-unit beds for COVID-19 patients. The hundreds of affected families were transferred to emergency shelters in schools, gyms, churches, boats, and courts. The previous record of the Acre River was reached in February 2012, reaching 3 cm below the 17.66 m level that was reached in March 1997.

A few months later, in June 2021, a new extreme flood was reported in the Rio Negro in Manaus. In fact, in 2021, in several municipalities in the Amazon basin, rivers reached levels higher than the maximum observed until then, making this year the biggest flood event in the entire history of monitoring [46]. The 2021 flood in Amazonia [50,51] was associated with an intensification of the atmospheric upward motion in the northern Amazonia (5° S–5° N) during austral summer and fall, which is related to an intensification of the Walker circulation. This atmospheric phenomenon is linked to an amplification of deep convective clouds and intense rainfall across northern Amazonia, leading to positive anomalies in terrestrial water storage during the 2021 austral summer. The strengthening of the Walker circulation corresponds to La Niña conditions, which have been associated with major floods in the Amazon during the 21st century (in 2009, 2012, and 2021). Additionally, in 2021, an intensification of the continental Hadley circulation was observed. These excessive rainfall patterns resulted in record-high water levels in the Rio Negro at Manaus, located in the central Brazilian Amazon, reaching the highest levels recorded in 102 years in June 2021, measuring 29.2 m [50].

3.2. Flow Rate Analyses

In Figure 4, the boxplot graph illustrates annual flow over 38 years. The obtained values reveal that the highest flow rate occurred in the year of 1995, which experienced a strong La Niña intensity (4430.433 m^3/s), and in 2008, a year of moderate La Niña (4559.125 m^3/s), followed by the year 2017, also a La Niña year (4430.433 m^3/s). The third-largest outlier was recorded in 2019 (4179.662 m^3/s). Conversely, 2019 marked the highest average flow and the most significant third quartile throughout the entire historical series.

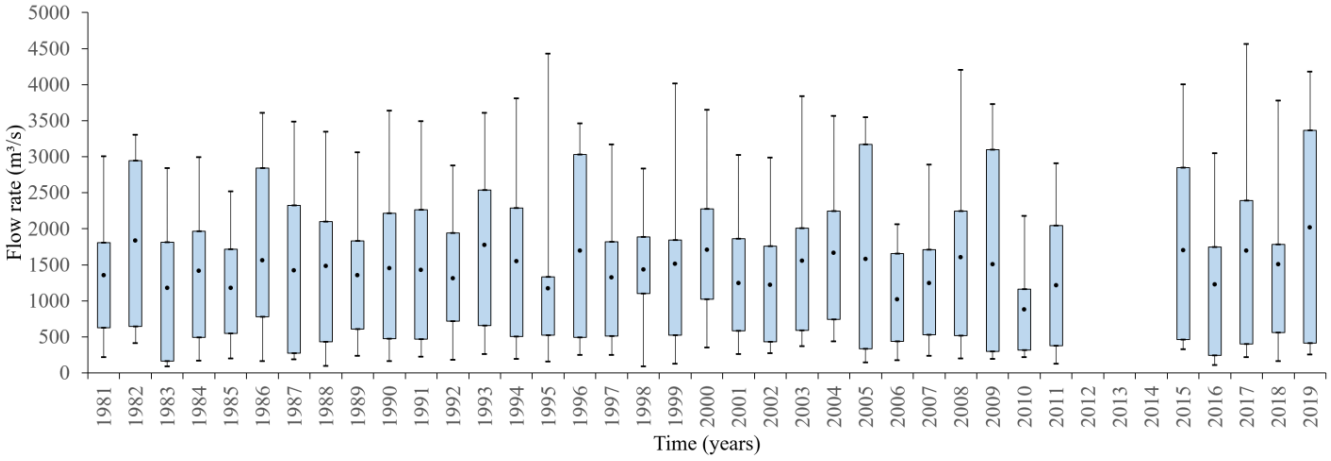

Figure 4. Flow rate time series (Source: Brazilian Water Agency, ANA).

The Dickey–Fuller test results show that the calculated p-value is $p = 0.285$, which is greater than the significance level $\alpha = 0.05$. The observed test statistic value is -2.562, and the critical value is -3.479. Therefore, the null hypothesis cannot be rejected. This implies that the time series of the flow rate is nonstationary. The risk of rejecting the null hypothesis while it is true is 28.52%. Hence, the statistical properties of the flow time series are changing over time, as indicated with this analysis.

The Durbin–Watson test indicates that the residuals of the flow time series are uncorrelated, as the calculated p-value of $p = 0.342$ is greater than the significance level $\alpha = 0.05$. With a DW statistic of 1.841 and $p = -0.747$, the risk of rejecting the null hypothesis while it is true is less than 3.95%. The Mann–Kendall test yields a calculated p-value that is lower than the significance level $\alpha = 0.05$. With Kendall's $\tau = 0.306$, $S' = 22$, and Var $(S') = 104$, with a two-tailed p-value of 0.039, the null hypothesis can be rejected, indicating that there is a trend in the flow rate time series. The risk of rejecting the null hypothesis while it is true is less than 3.95%. After applying the continuity correction, Sen's slope was calculated to be 192.264.

3.3. River Water Level Analyses

Analyzing river water levels is a crucial aspect of understanding hydrological patterns and their impacts on surrounding areas. The variation in water levels over time provides valuable insights into seasonal changes, flood events, and the potential risks they pose. In the case of the Juruá River, its water level fluctuations are notable due to the two distinct periods it experiences. During the winter months (December to May), the river enters a period of rising water levels, leading to flooding in the adjacent floodplain areas. This inundation can have significant consequences for nearby communities and infrastructure. Conversely, the summer months (June to November) witness a decline in water levels, making it challenging for larger vessels to navigate the river's middle course. This fluctuation has implications for transportation and trade activities in the region.

The boxplot in Figure 5a depicts the altimetric level of recorded water levels over 38 years. It is evident that only the years 1995 (14.12 m), 2017 (14.27 m), and 2019 (14.36 m) had considerably high maximum values, surpassing the overflow level (13.33 m). On the

other hand, the series exhibited a consistent behavior of outliers, with an average ranging between 8 and 10 m.

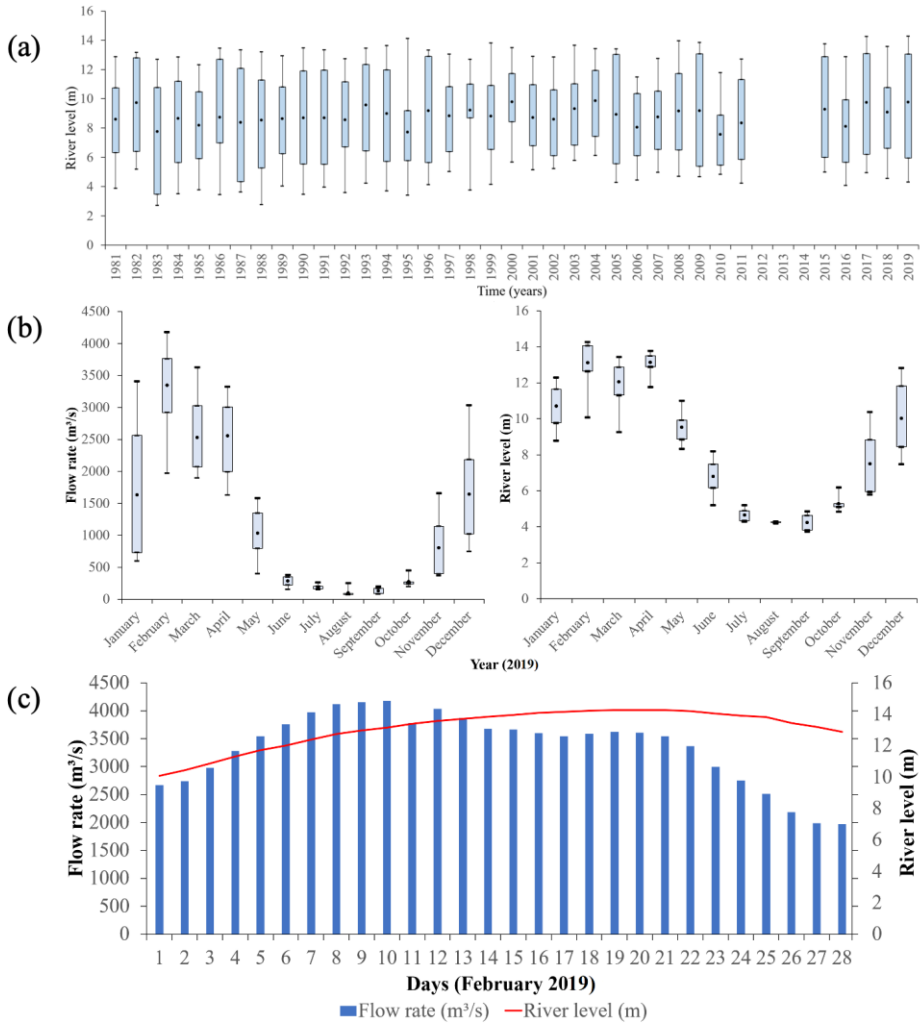

Figure 5. (**a**) River water-level time series. (**b**) Flow rate (m^3/s); river water-level data for 2019. (**c**) Daily flow rate and river water-level variability in February 2019.

The results of the Dickey–Fuller test indicated that the calculated *p*-value, $p = 0.285$, exceeds the significance level $\alpha = 0.05$. With an observed test statistic value of -2.562 and a critical value of -3.479, there is insufficient evidence to reject the null hypothesis. This suggests that the water level time series demonstrates nonstationary characteristics, implying changing statistical properties over time. Meanwhile, the Durbin–Watson test revealed that the residuals of the water level time series exhibit no correlation, as the calculated *p*-value of 0.268 is greater than the significance level $\alpha = 0.05$. The DW statistic of 0.54 and $p = 0.212$ result in a 34% probability of erroneously rejecting the true null hypothesis.

Additionally, the Mann–Kendall test demonstrated that the computed *p*-value is below the significance level $\alpha = 0.05$. With Kendall's $\tau = 0.278$, $S' = 20$, and Var (S') = 104, with a two-tailed *p*-value of 0.062, the null hypothesis can be rejected, indicating the presence of a trend in the water level time series. The risk of wrongly rejecting the null hypothesis while it holds true amounts to 6.24%. After applying the continuity correction, Sen's slope was determined to be 0.158.

Figure 5b presents the boxplot graph, depicting the flow values across different months of 2019. Notably, February emerges as the period of floods and inundations in Cruzeiro do Sul, with the highest flow values recorded. During this month, the flow reaches a maximum of 4179.662 m^3/s. Subsequently, other months follow this pattern: December

(3036.498 m^3/s), January (3410.247 m^3/s), March (3630.217 m^3/s), April (3325.323 m^3/s), and May (1585.018 m^3/s), collectively representing the rainy season of the region. Conversely, the months of June (380.736 m^3/s), July (262.719 m^3/s), August (254.266 m^3/s), September (202.846 m^3/s), and October (451.598 m^3/s) exhibit the lowest flows, indicative of the dry period in the region.

In the month of February, as a result, the river also exhibited the highest water level values, with an average of 13.10 m, a minimum value of 10.09 m, and a maximum value of 14.36 m recorded on the day of the event on the 19th. In Figure 5c, the boxplot graph depicts the daily flows and water levels. The average flow corresponds to 3346.453 m^3/s, the minimum value being 1971.036 m^3/s recorded on the 28th, and the maximum value of 4179.662 m^3/s recorded on the 10th. On the day of the event (19th), the flow was 3546.429 m^3/s. The higher water level values, above the overflow level (13 m), exhibit a maximum value of 14.36 m, followed by the months of April (13.78 m) and March (13.45 m). In August, the river exhibited its lowest water level at 4.3 m.

The highest water level that had been previously recorded was in 2017, reaching 14.24 m. The river's alert level is 11.80 m, and the overflow level is 13 m [51]. Although the flow value on the 19th was not the highest recorded, it marked the peak water level that the river had ever reached, surpassing the mark of 14.31 m, above the overflow level. This was considered the most significant flood ever recorded in this section of the Juruá River. Based on the results obtained and presented in the graph of Figure 5c, the flood map in Figure 6 is shown.

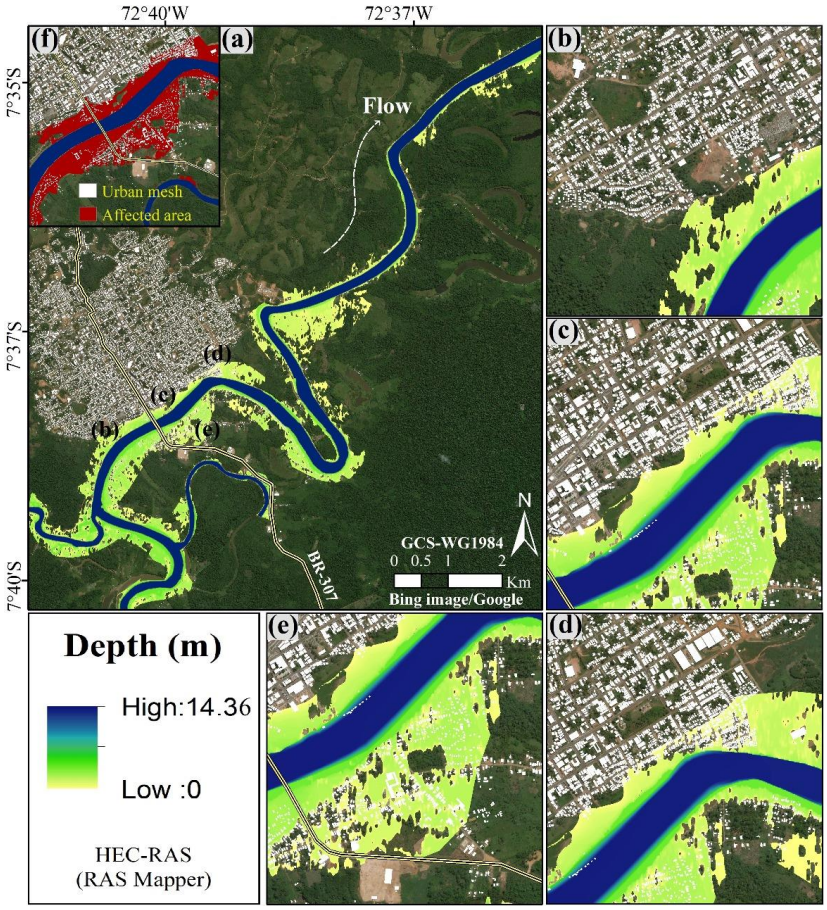

Figure 6. (**a**) Flood map of Cruzeiro do Sul and affected neighborhoods during the event on 19 February 2021. (**b**–**e**) indicate different areas of the river. (**f**) shows the urban area affected by the flood.

With the river exceeding the overflow level, the flood area mainly affects the urban area, both on the left bank and the right bank of the river. The flood area is not limited

only to the floodplain but also extends to adjacent areas along the river's course, including the highway BR-307 that provides access to Cruzeiro do Sul. The total flooded area is approximately 614.38 hectares.

From the graph in Figure 7, it can be observed that the areas most affected by the flood include urban areas, covering approximately 160.28 hectares, corresponding to 27% of the total affected area. Agricultural areas represent around 55% of the total affected area, with approximately 334.08 hectares. Meanwhile, areas covered by forests and grasslands, combined, account for about 17% of the total affected area, covering around 100 hectares.

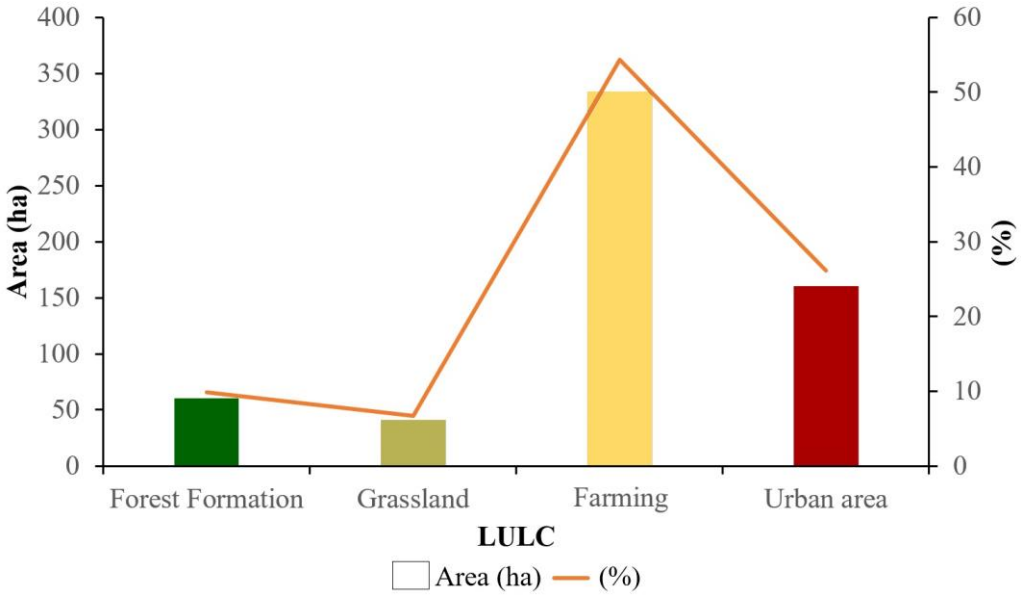

Figure 7. LULC area hit by the flood for the day of the event.

On the other hand, through the historical series, the analyzed data, along with literature reports, indicated that the latest extreme events in the municipality occurred in the years 1995, 2008, 2017, and 2021, all in the month of February and influenced by the La Niña phenomenon. This suggests that potentially predictable floods may or may not occur during this period, on a scale of around 10 years or more.

3.4. Flood Risk Mapping

The locations affected by the flood extent, with imminent risk, considering only urban areas, include the neighborhoods of Vila Cruzeirinho (Figure 8a), Centro (Figure 8b), Miritizal (Figure 8c), and Da Várzea (Figure 8d). As the flood extent expands, the risk areas, while primarily corresponding to the inhabited regions closest to the riverbanks due to the water level the water reaches, not only encompass the floodplain but also areas with moderate risk due to surface runoff.

Figure 9a illustrates the regions impacted in the risk map. It becomes evident that as the water level increases, triggered by the flow, the flooded area proportionally widens, resulting in an escalation of risk zones. Arranged in ascending sequence, the urban zones primarily affected, which exhibited elevated risks based on the simulated flood extension, fall under the "very low" risk category. This encompasses an approximate area of 24.07 hectares, constituting 7.86% of the total inundated expanse, at a water level of 13.33 m (0.3 m above the overflow threshold). Subsequently, the "low" risk classification encompasses around 47.85 hectares, corresponding to 29.32% of the complete area, with a water level of 13.6 m.

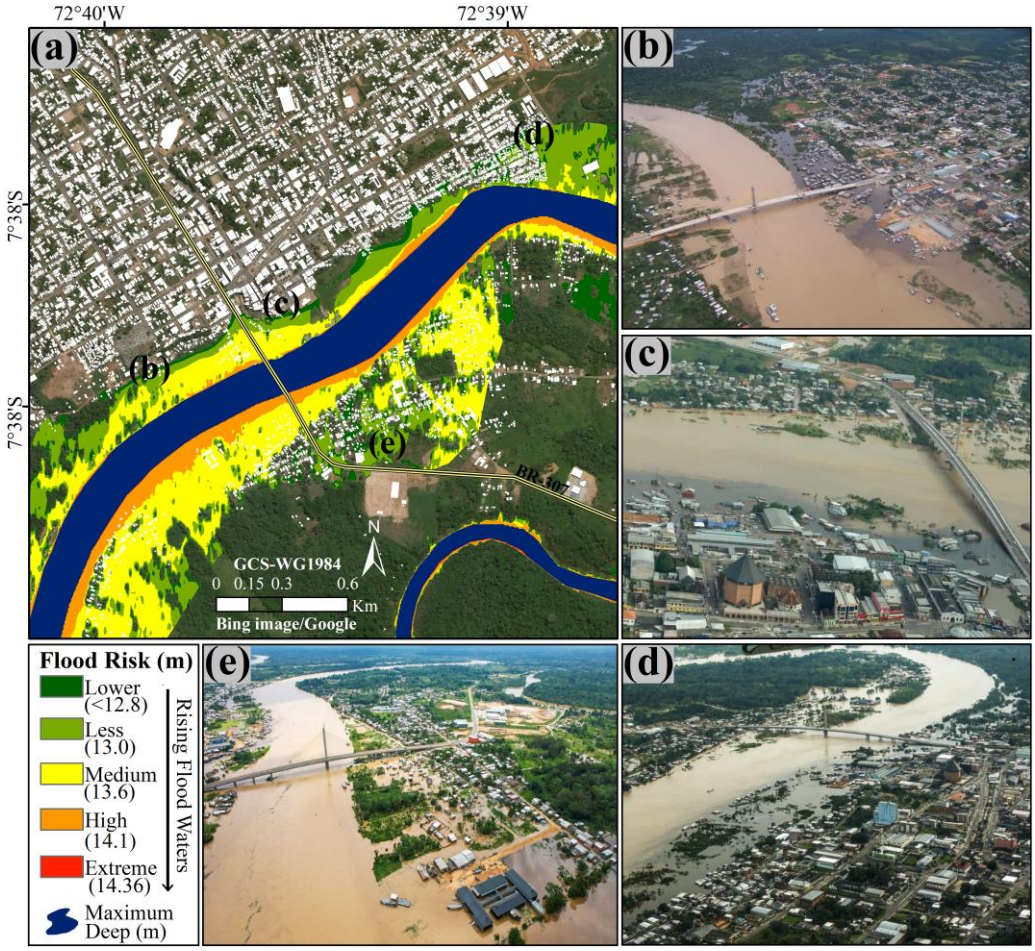

Figure 8. (**a**) Flood risk map; (**b**) Vila Cruzeirinho; (**c**) Centro; (**d**) Maritizal; and (**e**) Da Várzea.

Proceeding further, the subsequent category is the "moderate" risk class, characterized by a water level of 14 m. This encompasses an impacted expansion of 65.42 hectares, constituting roughly 41% of the entire affected area. Following this, the "high" risk class, positioned at a water level of 14.2 m, spans 25.53 hectares, constituting approximately 15.65% of the overall affected region. Lastly, the "very high" risk class, situated at a water level of 14.36 m, encompasses an area of roughly 0.27 hectares, representing a mere 0.16% of the total affected area.

Figure 9b displays the graphs of the simulated and observed time series at the ANA station, making it possible to observe that both exhibit similar behavior and values, with errors around 10% between these values, allowing us to ascertain that there is a correlation between the simulated and observed values. Thus, the statistical results obtained through the application of objective functions after model calibration are in accordance with the actual physical conditions of the river's behavior, enabling the attainment of reliable results for the simulated water levels that align with those observed at the station.

The Nash–Sutcliffe efficiency (NSE) validation score was 0.77. The NSE is a widely used statistic to assess the performance of hydrological or environmental models by comparing simulated values with observed data. In this case, an NSE value of 0.77 indicates that the model's predictions closely align with the observed data, capturing a significant portion of the variability in the system being studied. An NSE score of 0.77 implies that the model captures around 77% of the variance present in the observed data, which is considered a favorable result. The higher the NSE value, the better the model's performance in replicating the observed behavior. This validation score suggests that the model, in the context of the specific study or application, is providing reasonably accurate predictions.

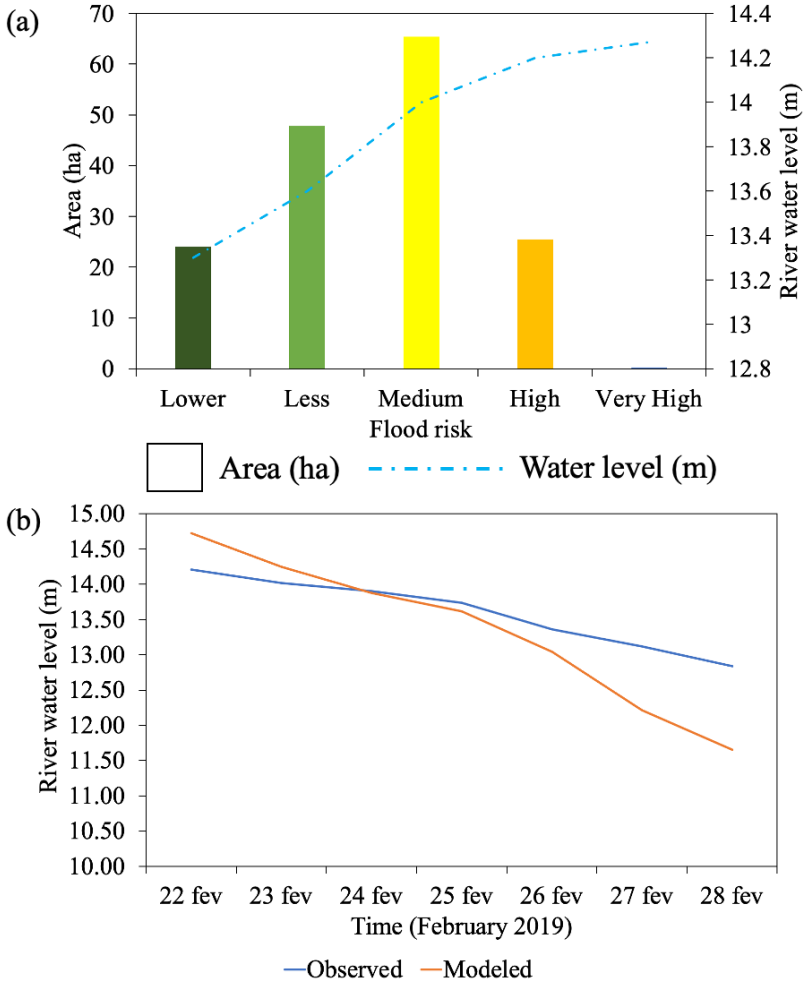

Figure 9. (**a**) Area of each class in relation with river water level. (**b**) River water level observed versus modeled.

The standard deviation ratio (RSR) value of 0.47 holds important implications for the variability and consistency of the data being analyzed. The RSR is a statistical metric used to assess the goodness-of-fit between observed and modeled data, particularly in the context of hydrological or environmental modeling. An RSR value of 0.47 suggests that the standard deviation of the residuals (the differences between observed and modeled values) is roughly 47% of the standard deviation of the observed data. In essence, an RSR value below 1.0 indicates that the variability in the model residuals is smaller than the variability in the observed data. This suggests a positive aspect of model performance, as a lower RSR value signifies a better fit between the modeled and observed values. An RSR value of 0.47 indicates a relatively strong agreement between the model's predictions and the observed data, with the model capturing a substantial portion of the data's variability.

A time-lagged frame can be seen in Figure 10. The river's alert level surged to 11.80 m on 2 February, indicating imminent danger with a lagged time frame for response. By 19 February, during the peak of the extreme event, the river soared to a staggering 14.31 m, causing widespread devastation. Fortunately, as the days progressed, the river level gradually receded, albeit still at a concerning 13 m by 25 February. This timeline illustrates the city's struggle against nature's relentless force, highlighting the resilience and adaptability of its inhabitants in the face of adversity.

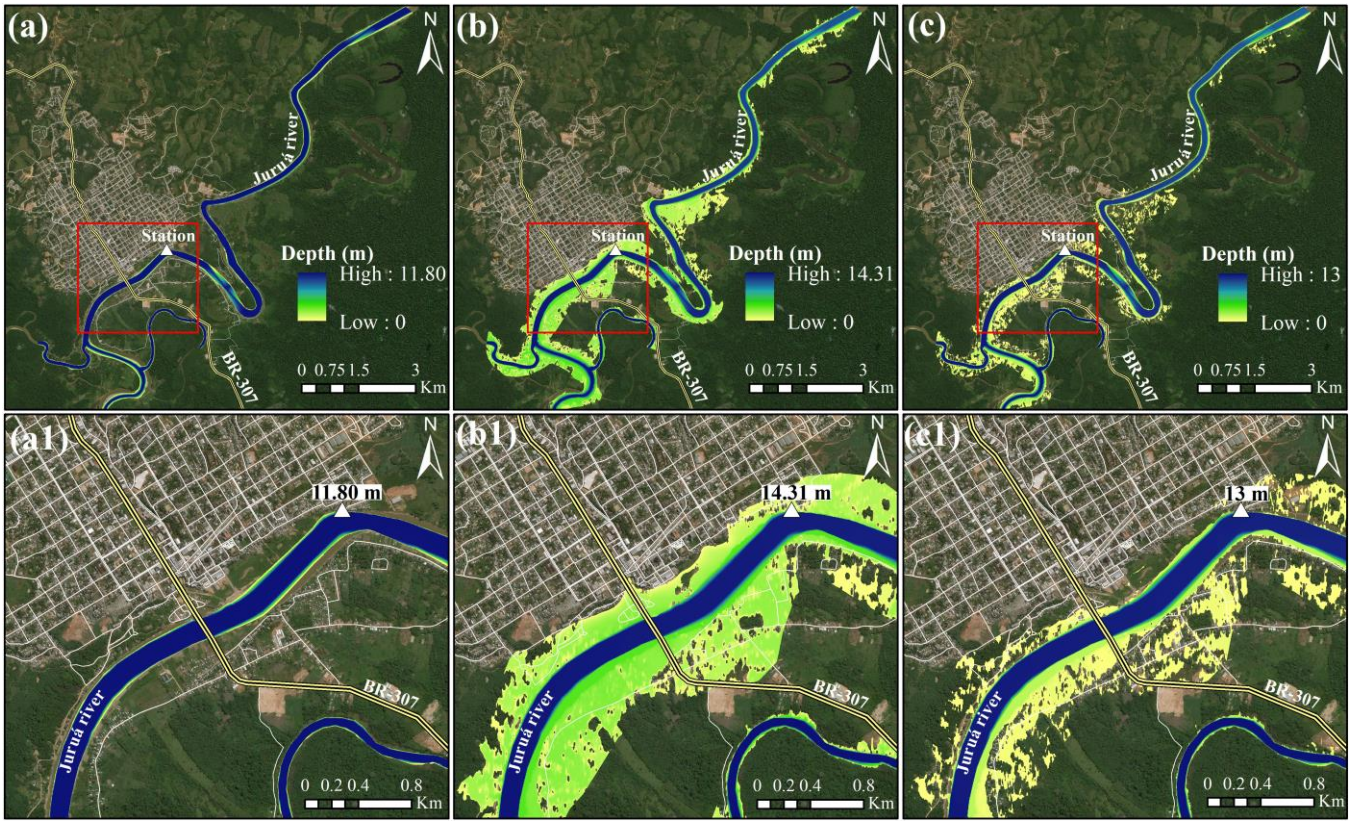

Figure 10. Flood map of Cruzeiro do Sul in February 2019: (**a**,**a1**) River alert level was 11.80 m on 2 February 2019; (**b**,**b1**) river level reached 14.31 m during the extreme event on 19 February 2019; and (**c**,**c1**) river level fell to 13 m on 25 February 2019.

4. Discussion

4.1. Flood Modeling Status

Floods pose significant threats to human lives, infrastructure, and the environment, necessitating continuous advancements in flood analysis techniques to enhance preparedness and resilience. Traditional flood analysis methods, such as statistical approaches and hydrological models, have limitations in accurately capturing complex flood dynamics. However, recent developments in remote sensing, machine learning, and hydroinformatics offer promising avenues for improving flood analysis capabilities. (1) With remote-sensing-based flood analysis, remote sensing technologies, including satellite imagery, airborne sensors, and unmanned aerial vehicles (UAVs), have revolutionized flood monitoring and mapping. Through providing high-resolution spatial data, remote sensing enables the identification of flood extent, depth, and dynamics with unprecedented accuracy. Studies [52,53] have demonstrated the effectiveness of satellite-based synthetic aperture radar (SAR) and optical imagery for flood detection and mapping in diverse environmental settings. (2) In machine learning approaches, machine learning algorithms, such as artificial neural networks (ANNs), support vector machines (SVMs), and random forests (RFs), have gained popularity for flood analysis due to their ability to learn complex patterns from data. Previous research showcases [54] the application of convolutional neural networks (CNNs) for flood detection using high-resolution satellite imagery, achieving superior performance compared to traditional methods. Similarly, [55] explores the use of ensemble learning techniques for flood forecasting, demonstrating improved prediction accuracy and reliability. (3) In hydroinformatics and data fusion, hydroinformatics integrates hydrological modeling, geospatial analysis, and data assimilation techniques to enhance flood analysis capabilities. By assimilating various data sources, such as gauge observations, remote sensing data, and numerical model outputs, hydroinformatics enables

comprehensive flood risk assessment and decision support. Contributions to this approach include [56], who developed a data fusion framework combining radar rainfall estimates and hydrological models for real-time flood forecasting. (4) Combining long hydroclimatic records with process-based models involves the compilation and analysis of extensive hydroclimatic datasets spanning multiple decades. These datasets encompass various meteorological, hydrological, and geomorphological parameters essential for understanding the complex dynamics of flood processes. Additionally, process-based models, such as hydrodynamic models and rainfall–runoff models, are employed to simulate flood events based on historical data inputs [57].

In many cases, an integrated approach that combines different methods can be the most effective for modeling flood occurrence and providing comprehensive information for risk management. It is important to consider the advantages and limitations of each method and tailor the modeling approach to the specific characteristics of the study area and project objectives. In the specific case of Cruzeiro do Sul, being an isolated area with limited data available, the approach used in this article was the most suitable.

4.2. Cruzeiro Do SUL Flooding

The flooding event that occurred in the city of Cruzeiro do Sul, Acre, Brazil, on 19 February 2019, stands as a significant example of the environmental challenges posed by recurring floods in the Amazon basin. The city's vulnerability to flooding is rooted in its geographical location, with its proximity to the Juruá River and the region's climatic conditions. This event not only underscores the immediate impacts of flooding but also highlights the importance of understanding the underlying causes, the spatial extent of the damage, and the implications for urban planning and disaster management to protect the population with the hope of making them more resilient to floods.

The occurrence of extreme floods in Cruzeiro do Sul is closely tied to the climatic and geographic features of the region. The city experiences distinct wet and dry seasons, with the rainy period extending from December to May, leading to inundations due to the overflow of the Juruá River. Conversely, the dry season from June to November results in lower water levels that restrict the navigation of larger vessels on the river. This cycle of inundation and recession plays a critical role in the region's agricultural activities, as the riverbanks are utilized by local farmers for cultivating crops such as beans, corn, potatoes, and watermelons [58].

The flood event of 19 February 2021 had significant consequences for the city's residents and infrastructure. While the flow value on this date was not the highest recorded, it marked the highest water level ever reached by the Juruá River, surpassing the previous peak recorded in 2017. The river's alert level is set at 11.80 m, with an overflow threshold at 13 m [58]. This flood event not only breached the overflow level but also had a far-reaching impact, encompassing not only the floodplain but also adjacent areas along the river's course. In the affected area, the transportation of medicine, food, and goods was made difficult, causing a cascade effect. The power shortages, mentioned above, can turn refrigerated food spoiled, causing more food supply problems.

An analysis of the flood's spatial distribution revealed that urban areas bore the brunt of the inundation, with agricultural and natural areas also significantly affected. As depicted in Figure 9, the areas most severely impacted covered approximately 27% urban, 55% agricultural, and 17% forest and grassland areas, respectively. Urban neighborhoods like Vila Cruzeirinho, Centro, Miritizal, and Da Várzea were found to be at imminent risk due to their proximity to the riverbanks and the consequent water level. While the highest risk was concentrated near the riverbanks, the expanding flood extent also extended to the moderate risk zones due to surface runoff. The proximity of urban livelihoods and flooded areas means a risk of water-related diseases, especially leptospirosis. Also, flooded areas combined with hot temperatures increases the speed of mosquitoes breeding, which favor outbreaks of vector borne diseases, such as malaria and dengue.

In Cruzeiro do Sul, the characteristics of urban areas at high risk of flooding can be influenced by various local and regional factors. Here are some considerations specific to this city: (a) Geographical location: Cruzeiro do Sul is situated near the Juruá River and other bodies of water, placing it in a region prone to flooding, especially during periods of heavy rainfall. (b) Topography and altitude: parts of the city may lie in low-lying areas relative to the river level, increasing the likelihood of flooding during intense or prolonged precipitation events. (c) Deforestation and urbanization: deforestation and haphazard urbanization around Cruzeiro do Sul may contribute to soil impermeability and increased surface runoff, exacerbating the risks of flooding. (d) Drainage systems: while Cruzeiro do Sul has drainage systems in place, these may be insufficient to cope with large volumes of water during extreme rainfall events. (e) History of flooding: the city may have a history of past floods, suggesting specific areas that are more prone to such events. (f) Population and economic concentration: Densely populated urban areas, especially those with critical infrastructure and significant economic activities, may be particularly vulnerable to floods due to potential damage to buildings, infrastructure, and livelihoods. (g) Limited resources and social inequalities: low-income populations in Cruzeiro do Sul may face additional challenges in preparing for, responding to, and recovering from flood events due to a lack of resources and limited access to services and protective infrastructure.

The lack of intensive-care-unit beds, mentioned above, worsens the response capacity to deal with those water-related and vector-borne diseases. This situation can be aggravated by the lodging of affected people in temporary shelters, which can contribute to the spread of the diseases. The lack of medicine, that should be transported by the flooded highway, can be one more factor for problems and difficulties. Cruzeiro do Sul is situated near rivers, including the Juruá River, which can overflow during periods of heavy rainfall. Mechanisms to mitigate (1) riverine flooding may include the following: (a) Early warning systems: implementation of systems to monitor river levels and provide timely alerts to residents in at-risk areas. (b) Floodplain management: zoning regulations and land-use planning to restrict development in flood-prone areas and preserve natural floodplains. (c) Infrastructure: construction of levees, embankments, and floodwalls to protect communities from river overflow. (d) Natural flood control: reforestation and restoration of riparian vegetation to reduce erosion and regulate water flow. (e) Community preparedness: education and training programs to raise awareness about flood risks and promote emergency preparedness among residents.

(2) Urbanization can exacerbate flooding in Cruzeiro do Sul by increasing the number of impervious surfaces and disrupting natural drainage patterns. Mechanisms to address urban flooding may include the following: (a) Stormwater management: implementation of drainage systems, retention ponds, and green infrastructure to capture and manage stormwater runoff. (b) Floodplain mapping: identification of areas prone to urban flooding to inform land-use planning and development regulations. (c) Sustainable urban design: adoption of design principles that promote permeable surfaces, green spaces, and water-sensitive urban planning. (d) Infrastructure upgrades: retrofitting of existing infrastructure, such as culverts and storm drains, to improve drainage capacity and reduce flood risk. (e) Building codes: enforcement of building codes to ensure that new construction is resilient to flooding and includes measures such as raised foundations and flood-resistant materials.

(3) Intense rainfall events can trigger flash floods, particularly in urban areas with poor drainage infrastructure. Mechanisms to address flash flooding may include the following: (a) Emergency response: establishment of rapid response teams and evacuation plans to protect residents during flash flood events. (b) Flood forecasting: use of weather forecasting models and radar systems to predict and anticipate flash flood events. (c) Green infrastructure: implementation of nature-based solutions such as rain gardens and permeable pavements to absorb and slow stormwater runoff. (d) Public awareness: public education campaigns to inform residents about the dangers of flash flooding and encourage proactive measures such as staying informed and avoiding flood-prone areas during heavy rainfall.

Policies aimed at addressing flooding in Cruzeiro do Sul may encompass a combination of these mechanisms, along with provisions for funding, coordination among government agencies, and engagement with stakeholders such as community organizations and private sector partners. Additionally, ongoing monitoring and evaluation of flood risk management efforts can inform adaptive strategies and ensure resilience to future flood events.

This event's aftermath underscores the necessity for robust flood mitigation strategies and informed urban planning. The evaluation of flood dynamics using geoprocessing, remote sensing, and hydraulic modeling, as exemplified in this study, can provide valuable insights for developing effective measures to alleviate the impact of such events. The flood maps generated offer a visual representation of risk areas and can guide land-use planning and construction practices to minimize the vulnerability of urban areas to flooding. Furthermore, the analysis of historical flood records and trends helps to predict potential flood occurrences in the future. Understanding that the 2019 flood event was associated with La Niña conditions, similar to other major floods in Amazonia during the 21st century, highlights the importance of early warning systems based on climate signals. This knowledge equips authorities and communities with the tools needed to prepare for and respond to potential flood events more effectively.

5. Conclusions

This study analyzed the flood dynamics in Cruzeiro do Sul, Brazil. Our assessment showed that the impact of flooding is not uniformly distributed, affecting urban areas by 27%, agricultural zones by 55%, and forest/grassland by 17%. Additionally, our research pinpointed high-risk urban neighborhoods—namely, Vila Cruzeirinho, Centro, Miritizal, and Da Várzea—that face escalating risks due to river proximity and surface runoff. This study also validated the recurring pattern of extreme floods occurring roughly every decade, specifically during La Niña events in February. These findings strongly underscore the need for integrated environmental planning and risk management, suggesting that a multipronged approach is essential to mitigate the far-reaching impacts of floods. Hence, this study serves as a cornerstone for future urban planning and policy formulation aimed at fostering sustainable and resilient practices in Cruzeiro do Sul.

Author Contributions: Conceptualization, J.M. and E.A.; methodology, J.M. and E.A; validation, J.M. and E.A.; formal analysis, J.M. and E.A.; investigation, J.M., E.A., J.A.M., L.L., E.P., A.P.C. and J.T.; resources, J.M. and E.A.; data curation, J.M. and E.A.; writing—original draft preparation, J.M., E.A., J.A.M., L.L., E.P., A.P.C. and J.T.; writing—review and editing, J.M., E.A., J.A.M., L.L., E.P., A.P.C. and J.T.; visualization, J.M., E.A., J.A.M., L.L., E.P., A.P.C. and J.T. All authors have read and agreed to the published version of the manuscript.

Funding: This research received funding from the Ministry of Education—Singapore (#Tier2 MOET2EP402A20-0001 and #Tier2 MOE-T2EP50222-0007).

Institutional Review Board Statement: Not applicable.

Informed Consent Statement: Not applicable.

Data Availability Statement: The data presented in this study are available on request from the corresponding author.

Acknowledgments: E.A. expresses sincere gratitude to CNPq (National Council for Scientific and Technological Development) for the grant of the research productivity fellowship.

Conflicts of Interest: The authors declare no conflicts of interest.

References

1. WHO. Climate Change. Available online: https://www.who.int/health-topics/climate-change#tab=tab_1 (accessed on 29 February 2024).
2. IPCC. *Climate Change, 2023. Synthesis Report. A Report of the Intergovernmental Panel on Climate Change. Contribution of Working Groups I, II and III to the Sixth Assessment Report of the Intergovernmental Panel on Climate Change*; Core Writing Team, Lee, H., Romero, J., Eds.; IPCC: Geneva, Switzerland, 2023.
3. IPT. *Instituto de Pesquisas Tecnológicas. Mapeamento de Riscos em Encostas e Margens de Rios*; Carvalho, C.S., Macedo, E.S., Ogura, A.T., Eds.; Ministério das Cidades/Instituto de Pesquisas Tecnológicas—IPT: São Paulo, Brazil, 2007; Available online: http://planodiretor.mprs.mp.br/arquivos/mapeamento.pdf (accessed on 18 May 2022).
4. Nimer, E. Clima. In *Geografia do Brasil: Região Norte*; IBGE: Rio de Janeiro, Brazil, 1977; Volume 1, pp. 39–58.
5. Poveda, G.; Waylen, P.R.; Pulwarty, R.S. Annual and inter-annual variability of the present climate in Northern South America and Southern Mesoamerica. *Palaeogeogr. Palaeoclimatol. Palaeoecol.* **2006**, *234*, 3–27. [CrossRef]
6. Garreaud, R.D.; Vuille, M.; Compagnucci, R.; Marengo, J. Present-day South American climate. *Palaeogeogr. Palaeoclimatol. Palaeoecol.* **2009**, *281*, 180–195. [CrossRef]
7. Győri, M.M.; Haidu, I.; Humbert, J. Deriving the floodplain in rural areas for high exceedance probability having limited data source. *Environ. Eng. Manag. J.* **2016**, *15*, 1879–1887. [CrossRef]
8. Vojtek, M.; Andrea, P.; Jana, V.; Shahla, A. Flood inundation mapping in small and ungauged basins: Sensitivity analysis using the EBA4SUB and HEC-RAS modeling approach. *Hydrol. Res.* **2019**, *50*, 1002–1019. [CrossRef]
9. Kim, D.; Lee, J.Y.; Yang, J.S.; Kim, J.W.; Kim, V.N.; Chang, H. The Architecture of SARS-CoV-2 Transcriptome. *Cell* **2020**, *181*, 914–921.e10. [CrossRef] [PubMed]
10. Manoranjan, M.; Rivas-Casado, M.; David, B. Understanding the effects of Digital Elevation Model resolution in urban fluvial flood modelling. *J. Hydrol.* **2021**, *596*, 126088. [CrossRef]
11. Costabile, P.; Costanzo, C.; De Lorenzo, G.; De Santis, R.; Penna, N.; Macchione, F. Terrestrial and airborne laser scanning and 2-D modelling for 3-D flood hazard maps in urban areas: New opportunities and perspectives Environ. *Environ. Model. Softw.* **2021**, *135*, 104889. [CrossRef]
12. Mantovani, J.R.; Bueno, G.T.; Alcântara, E.; Park, E.; Cunha, A.P.; Londe, L.; Marengo, J.A. Novel Landslide Susceptibility Mapping Based on Multi-criteria Decision-Making in Ouro Preto, Brazil. *J. Geovisualization Spat. Anal.* **2023**, *7*, 7. [CrossRef]
13. Marengo, J.A.; Alcantara, E.; Cunha, A.P.; Seluchi, M.E.; Nobre, C.A.; Dolif, G.; Goncalves, D.; Dias, M.A.; Cuartas, L.A.; Bender, F.; et al. Flash floods and landslides in the city of Recife, Northeast Brazil after heavy rain on May 25–28, 2022: Causes, impacts, and disaster preparedness. *Weather. Clim. Extrem.* **2023**, *39*, 100545. [CrossRef]
14. IBGE. Instituto Brasileiro de Geografia e Estatística. Available online: https://www.ibge.gov.br/en/geosciences/territorial-organization/territorial-organization/28114-malhas-de-setores-censitarios-divisoes-intramunicipais-2.html?lang=en-GB (accessed on 24 April 2023).
15. Ab'Saber, A.N. A organização natural das paisagens inter e subtropicais brasileiras. In *III Simpósio Sobre o Cerrado*; Ferri, M.G., Ed.; E. Blucher EDUSP: São Paulo, Brazil, 1971.
16. Köppen, W. Versuch einer Klassifikation der Klimate, vorzugweise nach ihren Beziehungen zur Pflanzenwelt. *Geogr. Z.* **1900**, *6*, 657–679.
17. Diretoria de Serviço Geográfico (DSG). *Banco de Dados Geográficos do Exército, Versão 5.0*; Diretoria de Serviço Geográfico (DSG): Brasília, Brazil, 2021.
18. Funk, C.; Peterson, P.; Landsfeld, M.; Pedreros, D.; Verdin, J.; Shukla, S.; Michaelsen, J. The climate hazards infrared precipitation with stations—A new environmental record for monitoring extremes. *Sci. Data* **2015**, *2*, 150066. [CrossRef] [PubMed]
19. Fuller, W.A. *Introduction to Statistical Time Series*, 2nd ed.; Wiley: Hoboken, NJ, USA, 1996.
20. Durbin, J.W.G.S. Testing for serial correlation in least squares regression: I. *Biometrika* **1950**, *37*, 409–428. [CrossRef] [PubMed]
21. Durbin, J.W.G.S. Testing for serial correlation in least squares regression: II. *Biometrika* **1951**, *38*, 159–179. [CrossRef] [PubMed]
22. Sen, P.K. Estimates of the regression coefficient based on Kendall's Tau. *J. Am. Statist. Assoc.* **1968**, *63*, 1379–1389. [CrossRef]
23. Rozante, J.R.D.S.; Moreira, L.G.G.; Goncalves De Vila, D.A. Combining TRMM and Surface Observations of Precipitation: Technique and Validation over South America. *Weather. Forecast.* **2010**, *25*, 885–894. [CrossRef]
24. Huffman, G.J.D.T.; Dan Braithwaite, R.; Bolvin, J.K.; Hsu Xie, P. Nasa Global Precipitation Measurement (Gpm) Integrated Multi-satellite retrievals for Gpm (Imerg). In *Algorithm Theor Basis Document (Atbd) Version, 2015*; NASA: Greenbelt, MD, USA, 2015.
25. MAPBIOMAS. Uso e Ocupação do Solo 2021, Coleção 6. 2022. Available online: https://mapbiomas.org/ (accessed on 17 October 2022).
26. USACE—U.S. *Army Corps of Engineers. HEC-RAS: User's Manual, Version 4.4.93*; Hydrologic Engineering Center (USACE): Davis, CA, USA, 2011.
27. USACE—U.S. *Army Corps of Engineers. HEC-RAS, River Analysis System Hydraulic Reference Manual, Version 4.1*; Hydrologic Engineering Center (HEC): Davis, CA, USA, 2010.

28. Hosseini, T.; Fathivand, A.; Barati, H.; Karimi, M. Assessment of radionuclides in imported foodstuffs in Iran. *J. Radiat. Res.* **2006**, *4*, 149–153.
29. Al-Zahrani, J. Estimation of Natural Radioactivity in Local and Imported Polished Granite Used as Building Materials in Saudi Arabia. *J. Radiat. Res. Appl. Sci.* **2017**, *10*, 241–245. [CrossRef]
30. United States Army Corps of Engineers (USACE). *HEC-RAS River Analysis System User's Manual*; Hydrologic Engineering Center: Davis, CA, USA, 2016.
31. Bates, P.D.; Horritt, M.S.; Fewtrell, T.J.; Wilson, M.D. Benchmarking urban flood models of varying complexity and scale using high resolution terrestrial LiDAR data. *Water Resour. Res.* **2010**, *46*, W09525.
32. Li, X.; Liu, H.; Tang, G.; Liu, X.; Fang, H. Comparison of HEC-RAS and MIKE21 for flood routing simulation: A case study of Wuhan in China. *Water* **2016**, *8*, 363.
33. Mohapatra, P.; Pandey, A. Flood Inundation Mapping using HEC-RAS and GIS: A Case Study in Mahanadi River Basin, Odisha, India. *Procedia Eng.* **2018**, *191*, 1079–1086.
34. Coulthard, T.J.; Neal, J.C.; Bates, P.D. Assessing the performance of a simplified flood inundation model. *J. Hydrol.* **2013**, *482*, 14–23.
35. Ponce, V.M.; Lugo, A. Modeling looped ratings in Muskingum-Cunge routing. *J. Hydrol. Eng. ASCE* **2001**, *6*, 119–124. [CrossRef]
36. Chow, V.T. *Open Channel Hydraulics*; Editora McGraw-Hill: New York, NY, USA, 1959; 680p.
37. Surwase, T.; Srinivasa, R.G.; Manjusree, P.; Begum, A.; Nagamani, V.; JaiSankar, G. Flood inundation simulation of Mahanadi River, Odisha during September 2008 by using HEC-RAS 2D model. In *Proceedings of the International Conference on Remote Sensing for Disaster Management*; Rao, P., Rao, K., Kubo, S., Eds.; Springer: Cham, Switzerland, 2019; pp. 851–863.
38. Mahdi, T.W.; Hillo, A.N.; Abdul-Sahib, A.A. Development and classification of flood hazard map using 2D hydraulic model. *IOP Conf. Ser. Mater. Sci. Eng.* **2021**, *1090*, 012122. [CrossRef]
39. Nash, J.E.; Sutcliffe, J.V. River Flow Forecasting through Conceptual Model. Part 1—A Discussion of Principles. *J. Hydrol.* **1970**, *10*, 282–290. [CrossRef]
40. Ritter, A.; Muñoz-Carpena, R. Performance evaluation of hydrological models: Statistical significance for reducing subjectivity in goodness-of-fit assessments. *J. Hydrol.* **2013**, *480*, 33–45. [CrossRef]
41. McCuen, R.H.; Knight, Z.; Cutter, A.G. Evaluation of the Nash–Sutcliffe efficiency index. *J. Hydrol. Eng.* **2006**, *11*, 597–602. [CrossRef]
42. Moriasi, D.N.; Arnold, J.G.; Van Liew, M.W.; Bingner, R.L.; Harmel, R.D.; Veith, T.L. Model Evaluation Guidelines for Systematic Quantification of Accuracy in Watershed Simulations. (PDF). *Trans. ASABE* **2007**, *50*, 885–900. [CrossRef]
43. Hyndman, R.J.; Koehler, A.B. Another look at measures of forecast accuracy. *Int. J. Forecast.* **2006**, *22*, 679–688. [CrossRef]
44. IPCC. *Climate Change 2022: Impacts, Adaptation and Vulnerability. Contribution of Working Group II to the Sixth Assessment Report of the Intergovernmental Panel on Climate Change*; Cambridge University Press: Cambridge, UK; New York, NY, USA, 2022; p. 3056. [CrossRef]
45. Marengo, J.A.; Jimenez, J.C.; Espinoza, J.C.; Cunha, A.P.; Aragão, L.E. Increased climate pressure on the agricultural frontier in the Eastern Amazonia–Cerrado transition zone. *Sci. Rep.* **2022**, *12*, 457. [CrossRef]
46. Cury, J.S.; Alves, L.G.S.; Oliveira, B.F.; Senna, R.C.; Albuquerque, B.S. 2021. What happened in 2021? Analyzing the biggest Negro River flood in Manaus, Brazil, Urban Water Systems & floods IV. *WIT Trans. Built Environ.* **2022**, *208*, 3–13.
47. Floodlist. 2021. Available online: https://floodlist.com/america/brazil-floods-acre-february-2021 (accessed on 18 May 2022).
48. Floodlist. 2021. Available online: https://floodlist.com/america/brazil-floods-acre-river-rio-branco (accessed on 18 May 2022).
49. Correio Braziliense. 2021. Available online: https://www.correiobraziliense.com.br/brasil/2021/02/4907832-com-enchente-dengue-e-covid-19-acre-chega-ao-6-dia-em-situacao-de-emergencia.html (accessed on 18 May 2022).
50. Espinoza, J.C.; Marengo, J.A.; Schongart, J.; Jimenez, J.C. The New Historical Flood of 2021 in the Amazon River Compared to Major Floods of the 21st Century: Atmospheric Features in the Context ofthe Intensif ication of Floods. *Weather. Clim. Extrem.* **2022**, *35*, 100406. [CrossRef]
51. Marengo, J.A.; Espinoza, J.C.; Alves, L.M.; Ronchail, J.; Cunha, A.P.; Ramos, A.M.; Molina-Carpio, J.; Correa, K.; Avalos, G.; Lavado-Casimiro, W.; et al. Central South America, in State of the Climate in 2021. *Bull. Amer. Meteor. Soc.* **2022**, *103*, S365–S368.
52. Bates, P.D.; Horritt, M.S.; Fewtrell, T.J. A novel approach to measuring urban flood dynamics using synthetic aperture radar. *J. Geovisualization Spat. Anal.* **2019**, *55*, 2311–2334.
53. Yan, K.; Liang, D.; Hong, Y. Flood inundation mapping using Sentinel-1 synthetic aperture radar data and convolutional neural networks. *J. Geovisualization Spat. Anal.* **2020**, *12*, 2762.
54. Liang, S.; Zhang, Y.; Wu, L. Flood detection in high-resolution satellite images using deep convolutional neural networks. *J. Geovisualization Spat. Anal.* **2021**, *596*, 126099.
55. Smith, J.; Brown, C.; Sampson, C. Ensemble learning for flood forecasting: A case study in data-scarce regions. *J. Geovisualization Spat. Anal.* **2022**, *24*, 123–138.
56. Gupta, H.V.; Bastola, S.; Sorooshian, S. A hydroinformatics framework for real-time flood forecasting using radar rainfall estimates. *J. Geovisualization Spat. Anal.* **2020**, *583*, 124584.

57. Fraehr, N.; Wang, Q.J.; Wu, W.; Nathan, R. Supercharging hydrodynamic inundation models for instant flood insight. *Nat. Water* **2023**, *1*, 835–843. [CrossRef]
58. Folha do Acre. 2021. Available online: https://folhadoacre.com.br/2021/03/05/enchente-gerou-prejuizo-de-r-300-milhoes-para-cerca-de-5-mil-pequenos-produtores/ (accessed on 18 May 2022).